Generating Antiaromaticity: Thermally-selective Skeletal Rearrangements at Interfaces

Elena Pérez-Elvira, Ana Barragán, Qifan Chen, Diego Soler-Polo, Ana Sánchez-Grande, Diego J. Vicent, Koen Lauwaet, José Santos, Pingo Mutombo, Jesús I. Mendieta-Moreno, Bruno de la Torre, José M. Gallego, Rodolfo Miranda, Nazario Martín, Pavel Jelínek, José I. Urgel, and David Écija

To cite this version

Pérez-Elvira, E; Barragán, A. *et al*. Generating Antiaromaticity: Thermally-selective Skeletal Rearrangements at Interfaces (2023).

https://repositorio.imdeananociencia.org/handle/20.500.12614/3379

Generating Antiaromaticity: Thermally-selective Skeletal Rearrangements at Interfaces

Elena Pérez-Elvira°[1], Ana Barragán°[1], Qifan Chen°[2,3], Diego Soler-Polo[2], Ana Sánchez-Grande[1,2,4], Diego J. Vicent[5], Koen Lauwaet[1], José Santos[5], Pingo Mutombo[2], Jesús I. Mendieta-Moreno[2], Bruno de la Torre[6], José M. Gallego[7], Rodolfo Miranda[1,4], Nazario Martín*[1,5], Pavel Jelínek*[2,6], José I. Urgel*[1], and David Écija*[1]

[1]IMDEA Nanoscience, C/ Faraday 9, Campus de Cantoblanco, 28049 Madrid, Spain
[2]Institute of Physics of the Czech Academy of Science, CZ-16253 Praha, Czech Republic
[3]Faculty of Mathematics and Physics, Charles University, V Holešovičkách 2, 180 00 Praha, Czech Republic
[4]Departamento de Física de la Materia Condensada, Universidad Autónoma de Madrid, 28049 Madrid, Spain
[5]Departamento de Química Orgánica, Facultad de Ciencias Químicas, Universidad Complutense de Madrid, 28040 Madrid, Spain
[6]Regional Centre of Advanced Technologies and Materials, Czech Advanced Technology and Research Institute (CATRIN), Palacký University Olomouc, 771 46 Olomouc, Czech Republic
[7]Instituto de Ciencia de Materiales de Madrid, CSIC, Cantoblanco, 28049 Madrid, Spain

° These authors contributed equally
* Address correspondence to these authors

Abstract

Antiaromatic polycyclic conjugated hydrocarbons (PCHs) are attractive research targets in modern organic chemistry in view of their interesting structural, electronic and magnetic properties. Unlike aromatic compounds, the synthesis of antiaromatic PHs is challenging as a result of their high reactivity and lack of stability, stemming from the small energy gap between their highest occupied and lowest unoccupied molecular orbitals. In this work, we describe a strategy toward the introduction of antiaromatic units in PHs *via* thermally selective intra- and intermolecular ring-rearrangement reactions of dibromomethylene-functionalized molecular precursors upon sublimation on a hot Au(111) metal surface, not available in solution chemistry. The synthetic value of these reactions is proven by 1) the integration of pentalene segments into acene-based precursors which undergo intramolecular ring-rearrangement; 2) the formation of π-conjugated ladder polymers, linked through cyclobutadiene connections, through ring-rearrangement and homocoupling reactions of indenofluorene-based precursors. The elucidation of the reaction products of the title reactions are investigated by scanning tunneling and non-contact atomic force microscopy investigations, and the mechanistic insights are unveiled by state-of-the-art computational studies.

1. Introduction

The concept of antiaromaticity was first introduced by Breslow in 1967 with the aim of explaining the usual instability of molecules with [4n] π-electrons in polycyclic conjugated systems[1,2]. In contrast to aromatic molecules[3], polycyclic conjugated hydrocarbons (PCHs) that follow the Hückel´s rule[4], antiaromatic PCHs present π-electron energies higher than that of their open-chain counterparts, turning them kinetically unstable and highly reactive[5]. In addition to the number of conjugated π-electrons within PCHs, the nature of their fragmental structures or subunits should also be considered for their aromatic (or antiaromatic) properties. Nowadays, antiaromatic and aromatic PCHs containing 4n π-subunits are attracting great interest as advanced materials for organic electronics and spintronics, due to a prevalent contribution of the antiaromatic segments to the overall topological, electronic and chemical properties of the PCHs[6]. In view of their high-lying highest occupied molecular orbital (HOMO) and low-lying lowest unoccupied molecular orbital (LUMO), such PCHs are considered as appealing research targets for small-molecule semiconductors[7,8], n-type materials[9,10] and organic secondary batteries[11]. For instance, structural modifications in linear acenes such as heteroatom replacement or the incorporation of non-benzenoid rings have recently gained increased attention as an alternative to acenes, which are susceptible to oxidation and dimerization under ambient conditions, reducing their aromaticity to achieve high charge mobilities[12–14]. Therefore, the development of stable compounds containing antiaromatic subunits is of utmost demand for further device application.

Modern methods in conventional organic chemistry have recently allowed the synthesis of several polycyclic antiaromatic systems, often requiring the attachment of bulky aryl substituents onto the most reactive sites of the molecule to attain a reasonable kinetic stability. During the last decade, on-surface synthesis has appeared as a profitable alternative to traditional organic chemistry, where the study of well-defined PCHs is reachable thanks to advanced scanning probe techniques, providing key mechanistic information on the reaction pathway[15,16]. The two-dimensional (2D) confinement of organic precursors together with the catalytic role of the underlying metal surface are primarily key factors of desirable or unexpected intramolecular reactions and intermolecular carbon-carbon (C–C) couplings, contributing to the expansion of the chemical toolbox of organic materials. Furthermore, additional controllable factors like precursor design, activation method, growth parameters, environmental conditions or substrate nature and symmetry, among others, should also be considered and properly tuned to steer the formation of the reaction products. As a result, a large number of chemical reactions have been successfully achieved on surfaces through non-conventional reaction mechanisms in the last years. For instance, members of the long-pursued acene[17–23], periacene[24–27], indenofluorene[28,29] or triangulene[30] families, as well as one-dimensional (1D) polymers that present expected[31] or unforeseen[32,33] C–C couplings have been recently achieved.

An innovative strategy toward the integration of antiaromatic units in PCHs is related to ring-rearrangement reactions. In this respect, thermal rearrangements, in which an atom, ion or chemical unit of a molecule is rearranged to obtain a structural isomer of the original molecule under a thermal stimulus, represents an excellent alternative to induce the formation of novel antiaromatic PCHs and conjugated polymers not accessible otherwise. Only recently, a few strain-induced rearrangement reactions of precursors that are composed of rigid and strained three dimensional (3D) structures have shown skeletal rearrangements in their backbone after planarization on metal surfaces[34–37]. In this respect, the selectivity of on-surface chemical reaction pathways is a promising approach to increase synthetic versatility, though remains largely underexplored[38]. Interestingly, thermal selectivity was confirmed in the case of competing intra- and intermolecular C–C couplings[39,40]. Although during the last years the on-surface synthesis of several antiaromatic PCHs[28,41,42] and polymers[43–49] has been reported, the systematic and well-defined introduction of antiaromatic segments into such carbon-based nanomaterials through skeletal ring-rearrangements, however, has been rarely achieved, and disruptive chemical strategies are necessary.

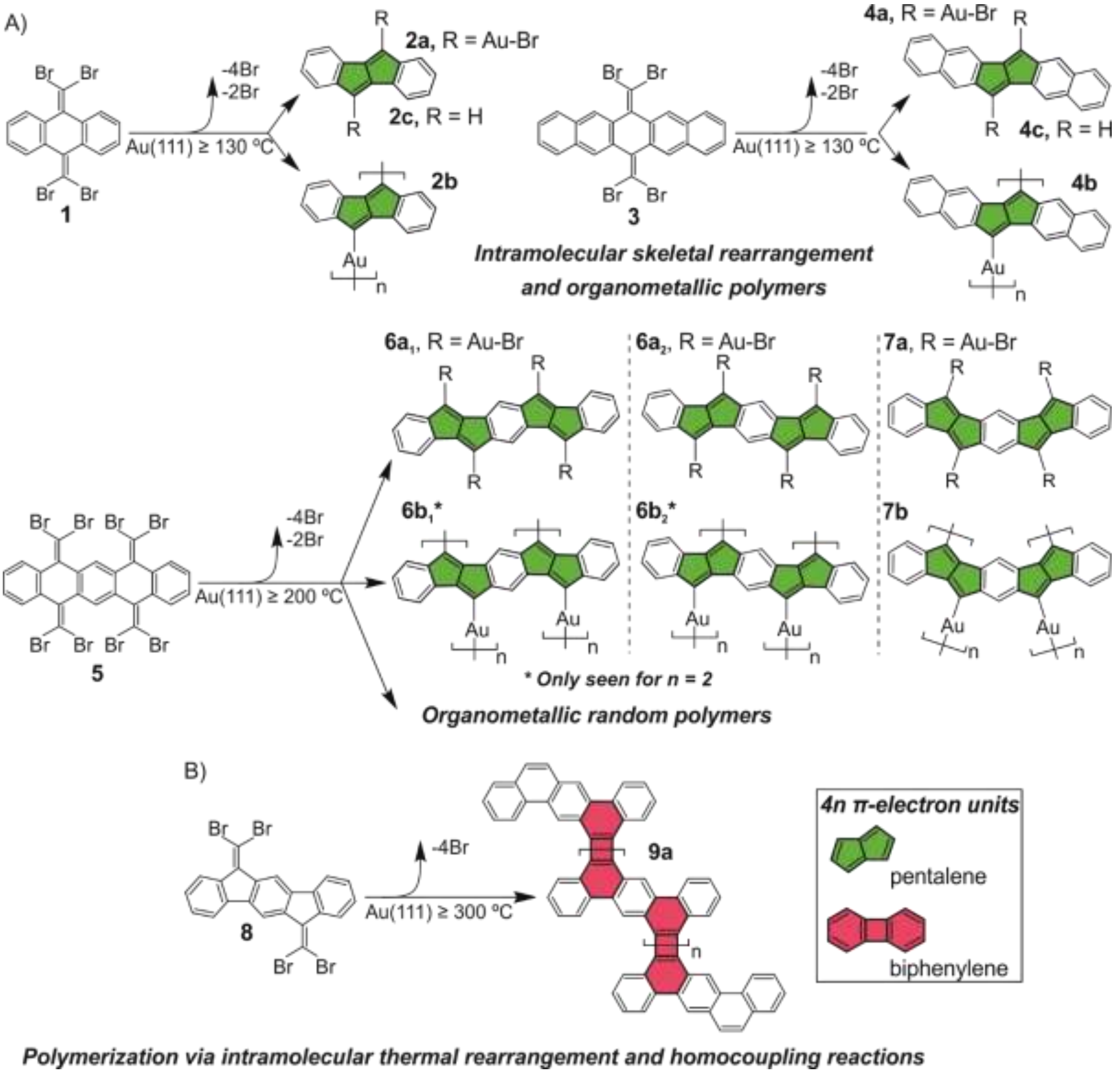

Scheme 1 | On-surface generation of antiaromatic subunits in PCHs and 1D polymers by a) Intramolecular thermal rearrangement and organometallic polymerization, and b) Intramolecular thermal rearrangement and subsequent homocoupling polymerization.

Herein, we introduce new routes toward the generation of antiaromatic segments into members of the acene and indenofluorene families through thermal rearrangement reactions on a metal surface. On one hand, intramolecular skeletal rearrangements induced the formation of diaceno[a,e]pentalenes after deposition of dibromomethylene-functionalized *p*-quinoid-based precursors on a hot Au(111) surface. In contrast, an analogous strategy on indenofluorene-based precursors, endowed with the same functional groups attached to the apical carbon of the five-membered rings, leads to the formation of π-conjugated ladder polymers of dibenz[*a*,*h*]anthracene units linked by cyclobutadiene segments (Scheme 1). Scanning tunneling microscopy (STM) and non-contact atomic force microscopy (nc-AFM) clearly unveil the chemical structure of the thermally activated intra- and intermolecular reactions. In addition, the experimental results are complemented by density functional theory (DFT) calculations, altogether providing a rationalization of the unique mechanisms driving reaction pathways.

2. Results and Discussion

Intramolecular thermal rearrangement reactions of dibromomethylene-functionalized p-quinoid-based acene precursors

The reaction illustrated in Scheme 1a provides a new strategy toward the transformation of pro-aromatic *p*-quinoid systems into pentalene antiaromatic systems. To explore this unique on-surface reaction, 9,10-bis(dibromomethylene)-9,10-dihydroanthracene precursor (**1**) was synthesized in solution. As recently shown by us for **1** and other dibromomethylene-functionalized precursors, the formation of ethynylene- or cumulene-bridged π-conjugated 1D polymers under ultrahigh vacuum (UHV) conditions on an Au(111) surface was demonstrated[50–56] by depositing a submonolayer coverage of the selected precursor on a surface held at room temperature, followed by an annealing process. In fact, upon thermal annealing of **1** (150 to 250 ºC), the molecular species dehalogenate and diffuse as surface-stabilized carbenes until they homocouple yielding an ethynylene-bridged anthracene polymer, where the aromatization of the quinoid precursors is ostensible[50]. However, a completely new scenario emerges when **1** is sublimed onto an already hot gold surface kept at 165 ºC. Instead of the previously found 1D molecular wires observed in STM images, individual asymmetric “cross-like” structures (**2a**) appear, surrounded by bright protrusions assigned to bromine (Br) atoms, which were dissociated from the precursor and bound to the gold substrate (Fig. 1a)[54,57,58]. Interestingly, high-resolution STM and nc-AFM images acquired with a carbon monoxide (CO)-functionalized tip allow to resolve their chemical structure[59] (Fig. 1b,c). In particular, constant-height frequency-shift images clearly show modifications in the molecular backbone, where a central pentalene moiety is flanked by two fused planar features assigned to two benzene rings, i.e. forming a dibenzo[*a*,*e*]pentalene derivative. Furthermore, **2a** presents bright lobes (Fig. 1b) or elongated straight lines (Fig. 1c) of an increased frequency shift, depending on the height of the recorded nc-AFM images, arising from the apexes of the five-membered rings that compose the pentalene subunit. This is attributed to the presence of Br atoms, still bonded to the molecular backbone, through a gold adatom, as elucidated below. The experimental features of such individual molecules are well reproduced by the DFT-optimized geometry (Fig. 1d) and the corresponding nc-AFM simulations[60] (Fig. 1e,f) on the Au(111) surface. Furthermore, analogous results are obtained for the sublimation of a fluorine-functionalized anthracene precursor on a hot Au(111) surface, i.e. 9,10-bis(dibromomethylene)-2,3,6,7-tetrafluoro-9,10-dihydroanthracene (see Fig. S1), demonstrating the versatility of the presented reaction toward modifications in the functionalization of the molecular backbone. The robustness of this individual asymmetric “cross-like” structures is confirmed by performing lateral manipulation experiments, which reveal that fluorinated Br−Au−dibenzo[*a*,*e*]pentalene molecules can be displaced and rotated along the gold surface (see Fig. S2).

Similar outcome is obtained upon the sublimation of a 9,10-bis (dibromomethylene)-9,10-dihydropentacene precursor (**3**) onto the gold surface kept at 200 ºC, resulting in the formation of Br−Au−dinaphtho[*a*,*e*]pentalene molecules (**4a**) (Fig. 2a-c).

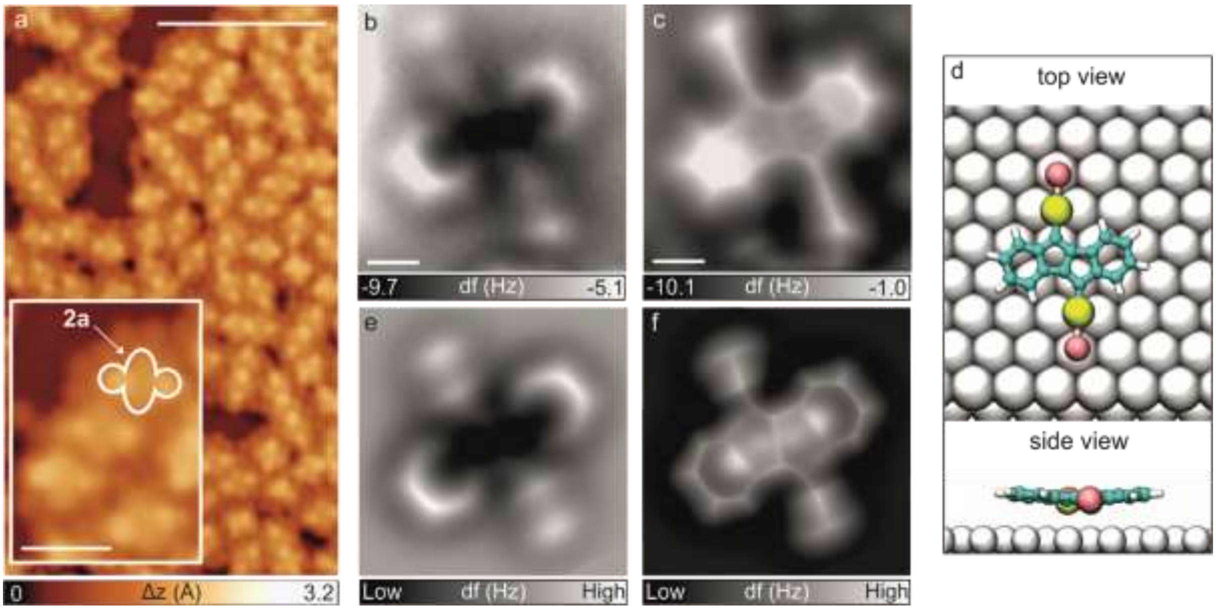

Fig. 1 | Integration of pentalene subunits in the molecular backbone of 1 by thermal rearrangement reactions upon deposition on a hot Au(111) surface. a, Overview STM topography image of the surface after sublimation of **1** on the Au(111) substrate kept at 165 °C, revealing the predominant presence of individual molecules surrounded by Br atoms. V_b = 0.2 V, I_t = 40 pA, scale bar: 5 nm. The inset depicts a high-resolution STM image where each molecule is composed of an elongated segment together with two brighter protrusions centered close to the transversal axis of the molecular backbone. **b-c,** Constant-height frequency-shift nc-AFM images of **2a** acquired with a CO-functionalized tip. The nc-AFM image shown in (c) was acquired 50 pm closer to the molecule than the nc-AFM image shown in (b), (z offset 90 pm above STM set point: 1 mV, 10 pA). Scale bars = 0.3 nm. **d,** Top and side views of the DFT equilibrium geometry of **2a** on Au(111). Atoms highlighted in light blue, yellow, red and white correspond to carbon, gold, bromine and hydrogen atoms respectively. **e-f,** Simulated nc-AFM images of panels (b) and (c), respectively. The simulated image displays in (f) is 0.5 Å closer to the substrate than (e).

Importantly, it is noticeable that an increase of the initial surface temperature induces a larger conversion of the precursors into diaceno[*a*,*e*]pentalenes, observing total conversion for surface temperatures of 200 ºC for **1** and 240 ºC for **3** (see graph in Fig. 2d). Thus, the thermal stimuli that the molecular precursors suffer upon absorption on the surface is crucial to drive the subsequent reaction pathways, switching from covalent polymerization (annealing from room temperature) to intramolecular ring-rearrangement reactions (adsorption on a hot substrate).

In addition to the observed dominant **2a** and **4a** species, different reaction products can be achieved after sublimation of both precursors at such temperatures in independent experiments. Notably, STM images reveal the appearance of new species, termed **4b**, visualized as chains connected through rounded protrusions (Fig. 2e). They are assigned to dinaphtho[*a*,*e*]pentalene organometallic oligomers with an observed intermolecular spacing of 2.2 ± 0.3 Å, which suggest a C−Au bond length of 2.1 ± 0.6 Å (see the Laplace filtered nc-AFM image in Fig. 2f), in agreement with previously reported works[17,61,62]. Comparable results are obtained for dibenzo[*a*,*e*]pentalene organometallic oligomers (**2b**) (see Fig. S3). Moreover, a small amount of individual dinaphtho[*a*,*e*]pentalene (**4c**) species could also be observed, i.e. without the Au-Br peripheral connections, being passivated by hydrogen residual gas present in the vacuum chamber, altogether giving a hint of the full reactivity scheme of the diaceno[*a*,*e*]pentalene molecules on surfaces. On the contrary, it was rare to find dibenzo[a,e]pentalene (**2c**) species (see Fig. S4 in SI).

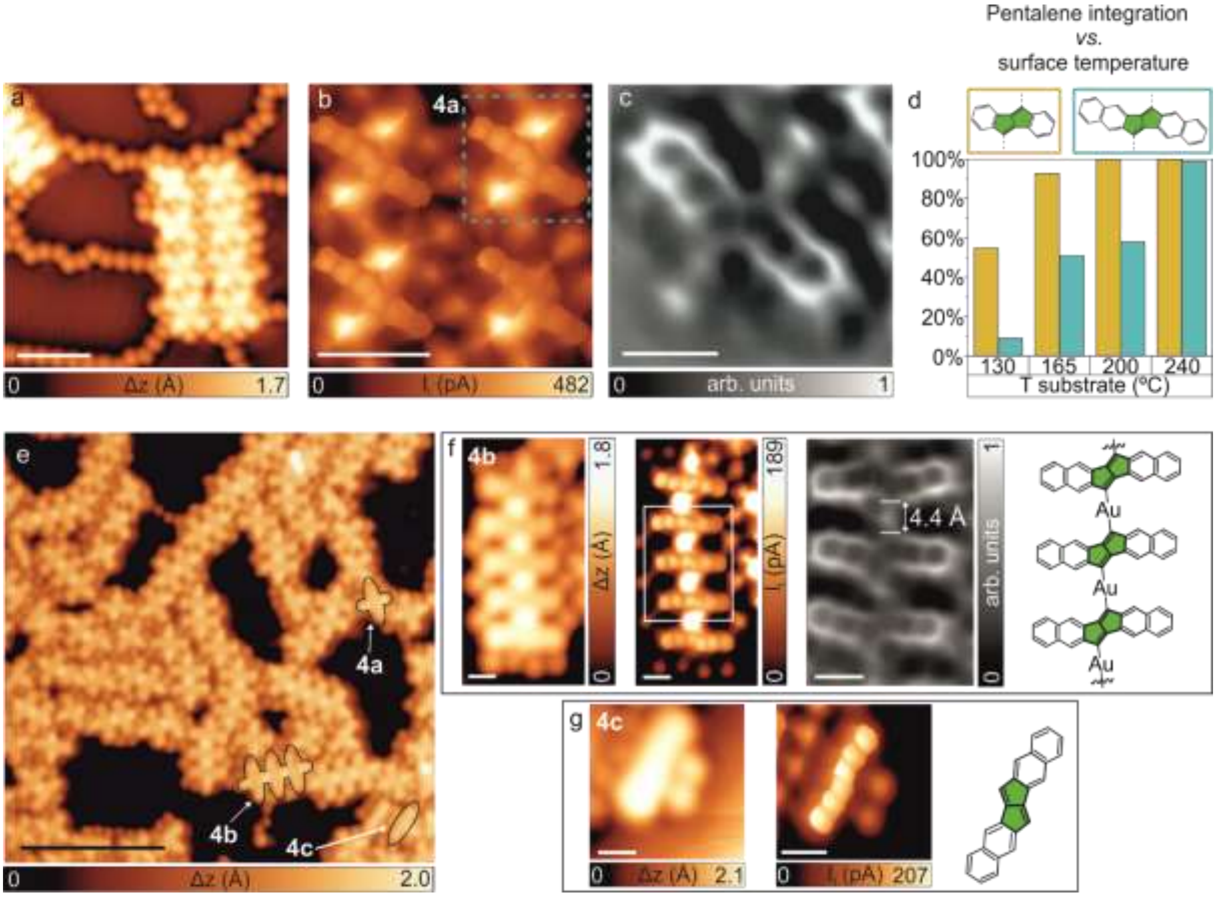

Fig. 2 | On-Surface synthesis of dinaphtho[a,e]pentalene derivatives. a, High-resolution image of the surface after sublimation of **3** on the Au(111) substrate kept at 200 °C. The sample reveals the predominant appearance of cross-like structures coexisting with cumulene-bridged π-conjugated pentacene polymers. V_b = -0.5 V, I_t = 40 pA, scale bar: 2 nm. **b,** Constant-height high-resolution STM image acquired with a CO-functionalized tip of four dinaphtho[a,e]pentalene molecules linked to two Br atoms per molecule through gold adatoms at the pentagonal apexes (**4a**). V_b = 5 mV, I_t = 40 pA, scale bar: 1 nm **c,** Laplace-filtered constant-height frequency-shift nc-AFM images of a molecule **4a** acquired with a CO-functionalized tip (z offset 90 pm above STM set point: 5 mV, 50 pA). Scale bar = 0.5 nm. **d,** Histogram depicting the integration of pentalene subunits in the molecular backbone of dibromomethylene-functionalized *p*-quinoid-based precursors (**1** and **3**) as a function of the substrate temperature. **e,** High-resolution image of the surface after sublimation of **3** on the Au(111) substrate kept at 200 °C. Notably, different dinaphtho[*a*,*e*]pentalene derivatives including those linked to two Br atoms per molecule through gold adatoms at the pentagonal apexes (**4a**), those forming gold organometallic oligomers (**4b**) and individual dinaphtho[*a*,*e*]pentalene molecules (**4c**) are observed. V_b = -0.5 V, I_t = 40 pA, scale bar: 5 nm. **f,** Constant-current and constant-height high-resolution STM images, together with a Laplace-filtered constant-height frequency-shift nc-AFM image and the corresponding chemical sketch of **4b**. Constant-current STM image: V_b = -0.5 V, I_t = 40 pA, scale bar: 0.5 nm. Constant-height STM image: V_b = 5 mV, I_t = 40 pA, scale bar: 0.5 nm. Constant-height frequency-shift nc-AFM image: z offset 35 pm below STM set point: 5 mV, 50 pA. Scale bar = 0.5 nm. **g,** Constant-current and constant-height high-resolution STM images along with the corresponding chemical sketch of an individual molecule **4c**. The pentalene subunits of the chemical sketches are colored in green to guide the reader. Constant-current STM image: V_b = -0.5 V, I_t = 40 pA, scale bar: 0.5 nm. Constant-height STM image: V_b = 5 mV, I_t = 40 pA, scale bar: 0.5 nm.

Next, in order to extend the number of antiaromatic subunits that can be integrated within a certain molecular backbone, we have sublimed a molecular precursor endowed with four dibromomethylene functional groups, namely 5,7,12,14-tetrakis(dibromomethylene)-5,7,12,14-tetrahydropentacene (**5**) on a gold surface kept at 200 ºC. In analogy to previous experiments involving precursors **1** and **3**, after the sublimation of a submonolayer coverage of precursor **5** on Au(111) held at 200 ºC, the intramolecular ring-rearrangement that gives rise to the integration of pentalene subunits was activated (see STM images in Fig. 3a). Such scenario is drastically different from the formation of indeno[1,2-b]fluorine π-conjugated polymers achieved by sublimation of the very same precursor **5** on Au(111) held at RT and subsequent annealing to 200 ºC[53].

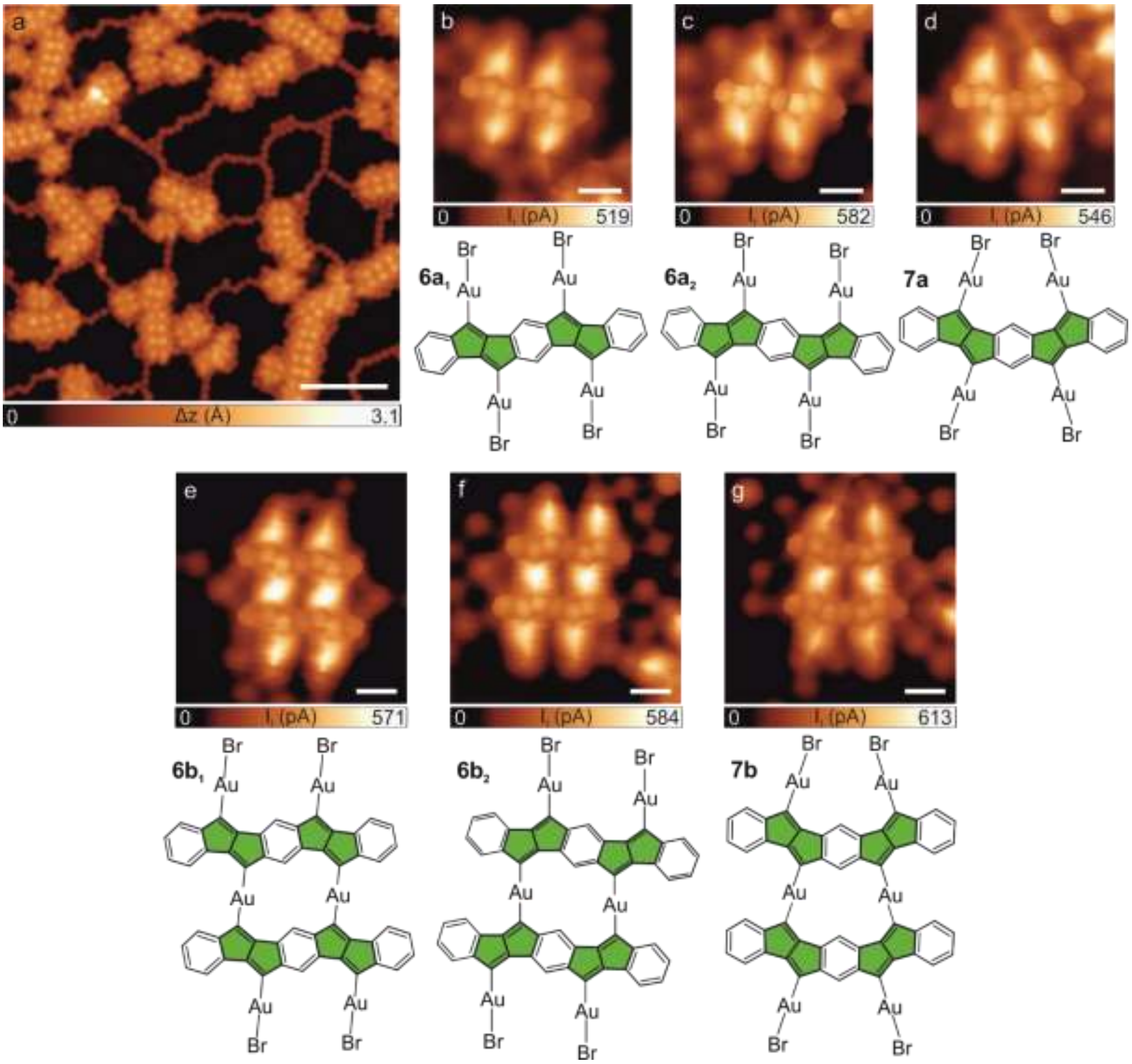

Fig. 3 | On-surface formation of diindeno[2,1-a:2',1'-g]-s-indacene, diindeno[2,1-a:1',2'-h]-s-indacene derivatives, and homochiral dimers through intramolecular ring-rearrangement reactions. **a,** Long-range STM topography image of the surface after sublimation of **5** on the Au(111) substrate kept at 200 °C. V_b = 0.5 V, I_t = 50 pA, scale bar: 5 nm. **b-d,** Constant-height high-resolution STM images acquired with a CO-functionalized tip and corresponding chemical sketches of **6a₁**, **6a₂** and **7a,** respectively. V_b = 5 mV, I_t = 50 pA, scale bar: 0.5 nm. **e-g,** Constant-height high-resolution STM image and corresponding chemical sketch of all three possible homochiral dimers **6b₁**, **6b₂** and **7b,** respectively, where the projected C−Au bond length of 2.2 ± 0.5 Å between both molecular backbones suggests the formation of organometallic oligomers, similar to those observed for **2b** and **4b**. V_b = 5 mV, I_t = 50 pA, scale bar: 0.5 nm.

Two distinct bispentalene-containing isomers were formed depending on the arrangement of the pentalenes with respect to the backbone[63–65]: a diindeno[2,1-*a*:2',1'-*g*]-s-indacene derivative, featuring two enantiomers upon adsorption on the surface, **6a$_1$** and **6a$_2$** (see Fig. 3b,c), and a diindeno[2,1-a:1',2'-h]-s-indacene derivative (**7a**) (see Fig. 3d). Again, the four elongated straight lines observed in the STM images are attributed to four Br atoms linked to the molecular backbone through gold adatoms. Coexisting with the individual species, organometallic oligomers of distinct length could be detected. Such oligomers are based on homochiral (see **6b$_1$**, **6b$_2$** and **7b** dimers in Fig. 3e-g and a hexamer of **7b** in Fig. S5a) or racemic combinations of the distinct bispentalene backbones (see Fig. S5 b-d). However, we could not find any hydrogenated counterparts. It should be noted that the length of the organometallic oligomers can vary ranging from two to six monomers under the mentioned reaction conditions, whereby 75% of the found species present one or two molecular units (statistics for ~500 molecules, see Fig. S6).

In addition, since we are introducing antiaromatic units into the precursor moieties, it is worth to theoretically analyze the aromaticity of the resulting species. To this aim, we have performed nucleus-independent chemical shifts (NICS) calculations, as well as the induced currents due to an applied magnetic field by analyzing the anisotropy of the induced current density (ACID) for products **2a**, **2c**, **4a**, and **4c** in the gas phase. As illustrated in Fig. S7, in the case of **2a** and **2c**, both NICS positive values of 26 and 38, respectively, as well as anti-clockwise ring current in the ACID plot indicate a strong antiaromatic character of the pentalene unit. For **4a** the antiaromatic character of pentalene unit is partially diminished by the presence of aromatic naphthalene moieties, exhibiting a NICS value of 16. On the contrary, in the case of **4c** the antiaromatic character of the pentalene is higher, displaying a NICS value of 30. For both **4a** and **4c**, a higher aromaticity is observed in the peripheral benzene units. Finally, it is worth to point out that benzannellation and naphthanellation of pentalene gives rise to an enhanced stability, affording relatively high HOMO-LUMO gaps between 2 and 3 eV,[66,67] while preserving the antiaromaticity of the pentalene moieties, though the measurement of their electronic structure on surfaces have remained elusive. To this aim, we have also paid attention to the electronic bandgap of an archetype of diaceno[a,e]pentalenes, i.e. the **4c** species. After sublimation of precursor **3** holding the substrate at 275 ºC being able to locate species **4c** are achieved, without concomitant bromine atoms, which have been desorbed[54]. As displayed in Fig. S8, by acquiring point STS on located positions of the compound, visualizing the spatial location of the frontier resonances by d*I*/d*V* mapping, and comparing the results with DFT calculations, we identify a bandgap of 3.1 eV, which is in the expected range for such compounds.

Reaction mechanism investigated by QM/MM calculations

To get further insights into the reaction mechanism that originates the generation of pentalene subunits in the molecular backbone of the 9,10-bis(dibromomethylene)-9,10-dihydroanthracene precursor (**1**), we carried out DFT and quantum mechanics/molecular mechanics (QM/MM) simulations.

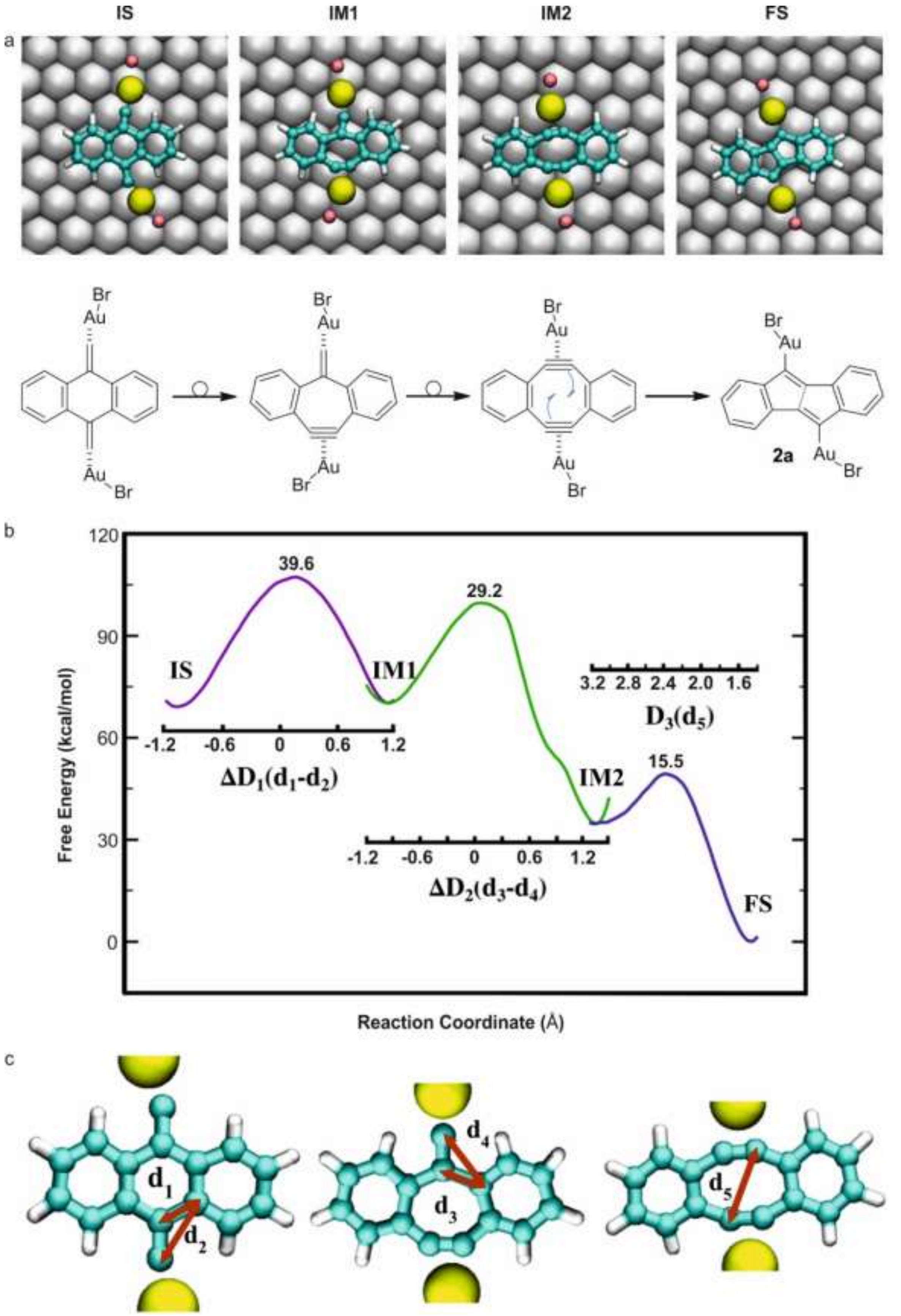

Fig. 4 | Free Energy Calculation of Surface-Catalyzed Reaction Pathways. a, Top view of the reaction snapshots and chemical schemes for initial state (IS), intermediate state 1 (IM1), intermediate state

2 (IM2) and final state (FS) at 227 ºC, respectively. The C, H, Br, Au adatom, and Au surface are represented in blue, white, pink, yellow, and gray balls, respectively. **b,** Free energy profile of the three-step reaction. The first part of the reaction goes through the reaction coordinate $\Delta D_1=d_1-d_2$, the second part through the reaction coordinate of $\Delta D_2=d_3-d_4$, while the third part from IM2 to FS using the single reaction coordinate of $D_3=d_5$. **c** Labels showing the atomic distances used in the definition of the reaction coordinates.

In a first step, a plausible scenario is the one where a gold adatom breaks one of the C-Br bonds of the precursor **1** and swaps positions with the Br atom forming a linear C-Au-Br complex, see Fig. S9. According to our QM/MM simulations, this process has relatively not only a low activation energy ~10 kcal/mol, but the product is also thermodynamically more stable. Next, molecular dynamics (MD) DFT simulations reveal that the debromination of the adjacent Br atom is thermodynamically favourable on the gold substrate, as shown in Fig. S10. This indicates that the Br atom not attached to a gold adatom can dissociate, thus yielding an intermediate structure containing a linear C-Au-Br complex, denoted as IS in Fig. 4a.

Fig. 4 shows a subsequent reaction course leading to the formation of the pentalene unit obtained from the free energy QM/MM simulations at 227 ºC. The reaction mechanism consists of several steps including two intermediate states (denoted as IM1 and IM2 in Fig. 4a). Herein, a carbon atom, bonded to the gold atom, incorporates into the central benzene ring, forming the intermediate structure IM1. This process has an activation energy 39.6 kcal/mol and the free energy of the intermediate IM1 is similar to the initial state, which makes this reaction step thermodynamically feasible. In the next step, the identical reaction mechanism takes place on the other side of the molecule forming the intermediate state IM2, see Fig. 4a. In this case the activation energy is even lower and the intermediate state IM2 is much more stable than IM1 (see Fig. S11). Notably, our QM/MM steered MD simulations show that these two reaction steps (globally, the transformation from IS to IM2 shown on Fig. 4a) occur indeed in a stepwise fashion rather than simultaneously (see video attached in the Supporting information). It is also worth mentioning the important role of the gold substrate in the reaction course. The presence of the gold substrate affects the relative stability of IM2 and the final state. Namely, without the gold substrate, the interaction of an Au atom in the C-Au-Br bonding complex would be much stronger and it would stabilize the organometallic complex, see Fig. S12. Thus, the reaction would not be thermodynamically feasible. This hints at the importance of the adatom-substrate interaction in the reaction process.

Once the intermediate IM2 is established, the final product with the pentalene unit can be formed with a very small activation barrier of 15.5 kcal/mol. Theoretically, also a final product with a four- and a six-membered ring could be alternatively formed, as shown in Fig. S13. However, according to our QM/MM free energy calculations, this product is much less stable.

Polymerization of dibromomethylene-functionalized indenofluorene-based precursors through intra-molecular thermal rearrangements and homocoupling reactions

In order to extend the general application of the above-mentioned strategy into not only intra-molecular ring-rearrangements, but also in the formation of π-conjugated polymers, we have performed experiments under comparable conditions using a dibromomethylene-functionalized indenofluorene precursor (**8** in Scheme 1b). STM images show that after sublimation of **8** on an Au(111) surface kept at 300 ºC, the spontaneous formation of 1D chains, coexisting with some concomitant fused segments is achieved (Fig. 5a). A closer look to these chains allows the clear identification of their chemical structure. The obtained high-resolution STM images

(Fig. 5b) together with the Laplace filtered constant-height frequency-shift image (Fig. 5c), using a CO-functionalized tip, reveal that the formed π-conjugated ladder polymer (**9a**) is constituted of planar dibenz[*a*,*h*]anthracene units connected through tetragons, attributed to cyclobutadiene moieties (see chemical sketch in Fig. 5c). This experimental finding is in contrast to the pentalene-linked indeno[1,2-*b*]fluorene polymers achieved by RT deposition of **8** and subsequent annealing to 350 ºC on the same surface (see Fig. S14)[54]. This type of connections is highly selective, being present in 85% of the analyzed segments (statistics out of 83 linkages).

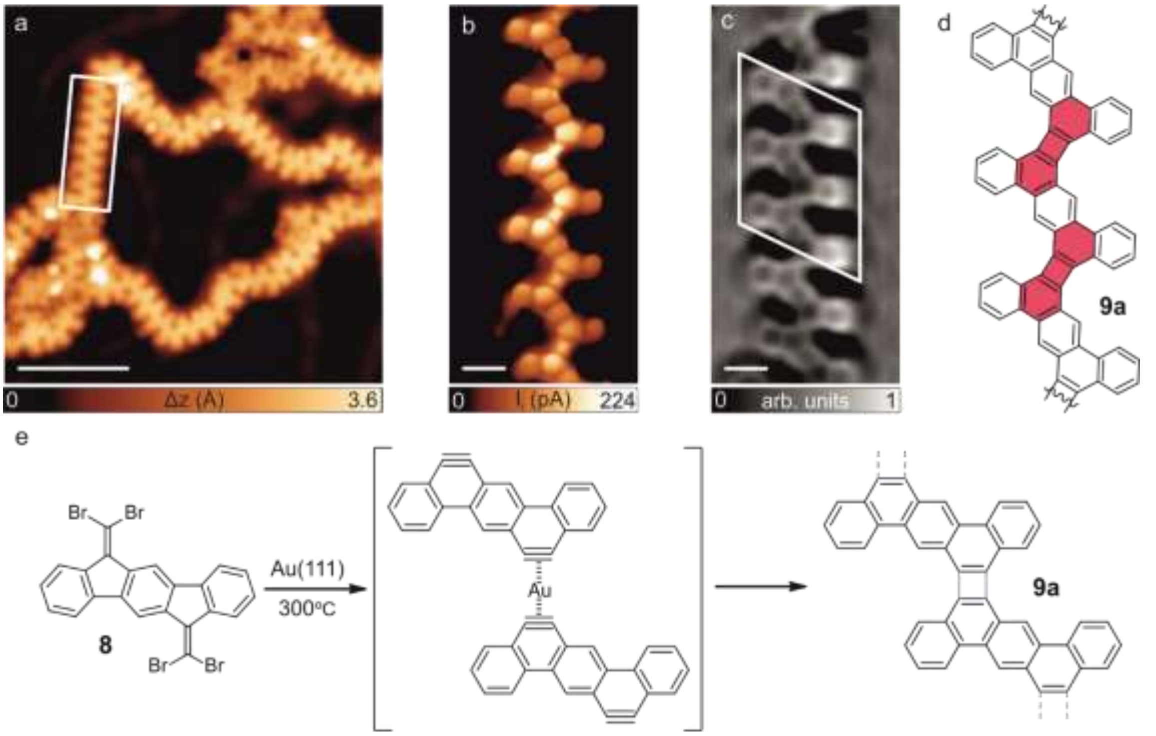

Fig. 5 | Polymerization of 8 via intra- and intermolecular thermal rearrangement reactions. a, Overview STM topography image after sublimation of **8** on the Au(111) substrate kept at 300 °C, reveals the formation of chains coexisting with some ill-defined segments. V_b = 0.1 V, I_t = 20 pA, scale bar: 5 nm. **b, c,** Constant-height high-resolution STM image and corresponding Laplace-filtered constant-height frequency-shift nc-AFM images acquired with a CO-functionalized tip of the segment of **9a** highlighted with the white rectangle in **a**. Herein, five dibenz[*a*,*h*]anthracene units connected each of them through tetragonal moieties is observed. **b:** V_b = 5 mV, I_t = 20 pA, scale bar: 0.5 nm. **c:** z offset 14 pm above STM set point: 5 mV, 50 pA). Scale bar = 0.5 nm. **d,** Chemical sketch of the segment highlighted by the white rhombus in **d**. The biphenylene subunits are colored in magenta to guide the reader. **e,** Proposed reaction mechanism toward the formation of **9a**.

Considering the huge computational cost that such a long series of reaction steps would require, we consider only a model case consisting of a single fluorene unit endowed with a dibromomethylene functional group, see Fig. S15. Such a simplified model can capture the main ingredients of the reaction mechanism. We assume that the first reaction step is similar to the previous case shown in Fig. 4, consisting of a partial debromination of the dibromo-methylene moiety and the formation of the linear C-Au-Br group *via* interaction with an Au adatom. The resulting intermediate, shown in upper right panel of Fig. S15, can be thermally activated to undergo an on-surface Fritsch-Buttenberg-Wiechell (FBW) rearrangement[68] leading to the formation of a benzyne moiety[38]. According to our QM/MM calculations the activation barrier is ~15 kcal/mol and the final product is thermodynamically more stable. Note, that the highly reactive intermediate is partially passivated by the presence of the Au-Br group. We tentatively assume that precursors equipped with two benzynes are formed, which later react with each other due to the presence of gold adatoms, giving rise to the observed **9a** polymers (see the proposed chemical reaction pathway in Fig. 5e). In addition, a residual amount (~15%) of dibenz[*a*,*h*]anthracene units linked by fused five membered rings (**9b**) are observed (see Fig. S16). The formation mechanism of these species **9b** is rationalized as a competing side-reaction of the homocoupling reaction (see Fig. S17), where the rearrangement of one hydrogen atom may generate a biradical species able to form a five-membered ring with a neighboring benzyne moiety.

Conclusions

Advancements in the field of on-surface synthesis demand new synthetic concepts and routes able to stimulate further research efforts and design innovative nanomaterials. Novel pathways toward the integration of antiaromatic subunits into PCH complexes, including polymers, is of special relevance since it can provide a wide variety of unprecedented extended π-systems with potential applications in organic materials/electronics. Here, we report the synthesis of PCHs and π-conjugated ladder polymers on a metal surface integrating, in a controllable fashion, [4n] π-electrons segments in the polycyclic conjugated backbone. Notably, all the reported compounds and polymers are unprecedented in solution chemistry or surface science. Combining high-resolution STM with nc-AFM for structural identification, with DFT and QM/MM based calculations for obtaining the reaction barriers has allowed for a complete elucidation of the reaction mechanisms. Sublimation of dibromomethylene-functionalized molecular precursors onto the hot Au(111) surface induces a spontaneous skeletal ring-rearrangement reaction. On the one hand, dibromomethylenes attached to six-membered rings of different precursors (**1** and **3**) lead to the formation of pentalene-based PCHs, i.e. diaceno[*a*,*e*]pentalenes (**2a,c** and **4a,c**) and their organometallic derivatives (**2b** and **4b**). Furthermore, the number of pentalene subunits introduced into a PCHs can be increased by an ingenious modification of the precursors (**5**), producing diindeno[2,1-*a*:2',1'-*g*]-s-indacene and diindeno[2,1-a:1',2'-h]-s-indacene PCHs (**$6a_1$/$6a_2$** and **7a**, respectively), as well as homochiral polymers of **7a** and random copolymers based on the racemic combination of **$6a_1$, $6a_2$** and **7a**. On the other hand, for dibromomethylenes attached to five-membered rings (**8**) sublimed onto a hot gold surface, π-conjugated ladder polymers linked through cyclobutadiene bridges are formed upon ring-rearrangement of the fulvene carbene segments to give a benzyne that, thereafter, undergoes a coupling reaction with a neighboring benzyne moiety (**9a**). Thus, the synthetic strategies presented in this work provide the basis of the syntheses of π-systems introducing antiaromatic subunits, which can serve as a good platform to design novel spintronics and optoelectronics devices. Furthermore, our work anticipates further research efforts to elucidate the influence of thermal stimuli in the reaction pathways of on-surface synthesis.

3. Methods

STM and nc-AFM experiments

Experiments were performed in two independent custom-designed ultra-high vacuum systems (base pressure below 5×10^{-10} mbar) hosting commercial low-temperature microscopes with STM/AFM capabilities from Scienta Omicron and Createc GmbH. The Au(111) substrate (MaTeck GmbH) was cleaned by repeated cycles of Ar^+ ion sputtering (E = 1 keV) and subsequent annealing to 740 K for 10 minutes. All STM images shown were taken in constant current mode, unless otherwise noted, with electrochemically etched tungsten and Pt/Ir tips, at a sample temperature of 4.3 K (Omicron) and 4.2 K in a custom designed LT-STM/nc-AFM system (Createc GmbH), respectively. Scanning parameters are specified in each figure caption. Molecular precursor **1**, **3**, **5** and **8** were thermally sublimed onto clean Au(111) or Au(111)/Mica substrates, kept at a temperature specified in the text, with a typical deposition rate of 0.5 Å/min (sublimation temperatures of 100, 160, 230 and 195 °C, respectively). The surface temperature was measured by a thermocouple contact on the sample plate. Non-contact AFM measurements were performed with a tungsten or a Pt/Ir tip attached to a Qplus tuning fork sensor.[69] The tip was a posteriori functionalized by a controlled adsorption of a single CO molecule at the tip apex from a previously CO-dosed surface.[70] The functionalized tip enables the imaging of the intramolecular structure of organic molecules.[59] The sensors were driven at their resonance frequency (26/30 kHz) with a constant amplitude of ~60/50 pm in both the Scienta Omicron and Createc GmbH instruments. The frequency shift from resonance of the sensor (with the attached CO-functionalized tip) was recorded in a constant-height mode (Omicron Matrix electronics and MFLi PLL by Zurich Instruments for Omicron; Nanonis SPM controller with Nanonis OC4 forCreatec GmbH). The STM and nc-AFM images were analyzed using WSxM.[71]

Computational details

We have used the Fireball/AMBER software to simulate the QM/MM Molecular Dynamics of the chemical reactions. To define the forces of the classical part (which consist in the most part of the metal surface) we employ the interface force-field and the dynamics is controlled by the AMBER code[72,73]. The quantum region is treated at the BLYP-DFT level with the Fireball software[74], a local-orbital DFT code which employs an optimized basis set of pseudo-atomic orbitals. The interface between Fireball and AMBER was implemented and described in[75].

We have employed a combination of Umbrella Sampling Simulations (US)[76] and Steered Molecular Dynamics (SMD)[77] to unveil the features of the reaction mechanism and calculate the free energy profiles of the reactions.

Before the US or SMD, we have performed a QM/MM geometry optimization followed by a thermalization from 300K to 500 K in order to stabilize the system. We use the Langevin thermostat as implemented in AMBER[78] to simulate the canonical ensemble. We use the Alan Grossfield´s implementation[79] for the Weighted Histogram Analysis Method (WHAM)[80] to calculate Free Energy profiles associated to each reaction from the US. See the paragraph on the reaction mechanism of the previous section for more information about the reaction coordinates on each case. On each of these cases, an initial SMD is employed to drag the corresponding reaction coordinate and generate structures which can be used as seeds for each US window. To construct the free energy profile, we made 121 umbrella sampling windows from -1.20 Å to 1.20 Å for the ΔD_1 (d_1-d_2) combined reaction coordinate from the Initial State (IS) to the Intermediate State 1 (IM1) and 141 windows from -1.20 Å to 1.50 Å for the ΔD_2 (d_3-d_4) combined reaction coordinate from the IM1 to the Intermediate State 2 (IM2), while for the reaction pathway from IM2 to the Final State (FS), the free energy is reconstructed by 81 umbrella sampling windows from 3.00 Å to 1.40 Å using a single reaction coordinate $D_3 = d_5$. Each US window is a QM/MM Molecular Dynamics of 10000 steps at 500K with a time step of 0.5 fs.

Theoretical d*I*/d*V* maps were calculated by the Probe Particle Scanning Probe Microscopy (PP-STM) code[81] for a metallic tip, which was represented by s-like orbitals. Anisotropy of the Induced Current Density (ACID)[82] and nuclear induced chemical shift (NICS)[83] was calculated in Gaussian16 package[84] [ref4] at UB3LYP/def2-SVP[85] level of theory and plotted using the code AICD version 3.0.3. Only π-orbitals were included in the calculation.

4. Acknowledgements

This project has received funding from Comunidad de Madrid [projects QUIMTRONIC-CM (Y2018/NMT-4783) and NanoMagCost (P2018/NMT-4321)], ERC Consolidator Grant (ELEC-NANO, 766555), ERC (SyG TOMATTO ERC-2020-951224), and Ministerio de Ciencia, Innovacion y Universidades (projects SpOrQuMat (PGC2018-098613-B-C21), CTQ2017-83531-R, PID2019-108532GB-I00, PID2020-114653RB-I00 and CTQ2016-81911-REDT). This study was also supported by MCIN with funding from European Union NextGenerationEU (PRTR-C17.I1) (MAD2D-CM)-MRR project. IMDEA Nanociencia is appreciative of support from the "Severo Ochoa" Programme for Centers of Excellence in R&D (MINECO, grants SEV-2016-0686 and CEX2020-001039-S). Q.C, D.S. and P.J. acknowledge funding support from the CzechNanoLab Research Infrastructure supported by MEYS CR (LM2023051) and GACR project no. 20-13692X. Computational resources were provided by the e-INFRA CZ project (ID: 90140), supported by the Ministry of Education, Youth and Sports of the Czech Republic. A.S-G thanks the funding from the "Ministerio de Universidades" for the "Plan de Recuperación, Transformación y Resiliencia" under the Margarita Salas grant agreement CA1/RSUE/2021-00369. J.I.U. acknowledges the European Union's Horizon 2020 research and innovation programme under the Marie Skłodowska-Curie grant agreement No [886314]. We acknowledge Dr. Borja Cirera for fruitful discussions.

5. Data and Code Availability

The datasets generated during and/or analyzed during the current study are available from the corresponding author on reasonable request. The Fireball software package is available at: https://github.com/fireball-QMD and PP-SPM software package can be downloaded at: https://github.com/Probe-Particle/ppafm#probe-particle-model.

6. References

1. Breslow, Ronald., Brown, John. & Gajewski, J. J. Antiaromaticity of cyclopropenyl anions. *J. Am. Chem. Soc.* **89**, 4383–4390 (1967).
2. Breslow, R. Antiaromaticity. *Acc. Chem. Res.* **6**, 393–398 (1973).
3. Randic, M. Aromaticity and conjugation. *J. Am. Chem. Soc.* **99**, 444–450 (1977).
4. von E. Doering, W. & Detert, F. L. CYCLOHEPTATRIENYLIUM OXIDE. *J. Am. Chem. Soc.* **73**, 876–877 (1951).

5. Zeng, Z. *et al.* Pro-aromatic and anti-aromatic π-conjugated molecules: an irresistible wish to be diradicals. *Chem. Soc. Rev.* **44**, 6578–6596 (2015).
6. Cao, J. *et al.* The Impact of Antiaromatic Subunits in [4n+2] π-Systems: Bispentalenes with [4n+2] π-Electron Perimeters and Antiaromatic Character. *J. Am. Chem. Soc.* **137**, 7178–7188 (2015).
7. Kawase, T. *et al.* Dinaphthopentalenes: Pentalene Derivatives for Organic Thin-Film Transistors. *Angew. Chem.* **122**, 7894–7898 (2010).
8. Chase, D. T. *et al.* 6,12-Diarylindeno[1,2-b]fluorenes: Syntheses, Photophysics, and Ambipolar OFETs. *J. Am. Chem. Soc.* **134**, 10349–10352 (2012).
9. Dai, G., Chang, J., Jing, L. & Chi, C. Diacenopentalene dicarboximides as new n-type organic semiconductors for field-effect transistors. *J. Mater. Chem. C* **4**, 8758–8764 (2016).
10. Grenz, D. C., Schmidt, M., Kratzert, D. & Esser, B. Dibenzo[*a* , *e*]pentalenes with Low-Lying LUMO Energy Levels as Potential n-Type Materials. *J. Org. Chem.* **83**, 656–663 (2018).
11. Shin, J.-Y., Yamada, T., Yoshikawa, H., Awaga, K. & Shinokubo, H. An Antiaromatic Electrode-Active Material Enabling High Capacity and Stable Performance of Rechargeable Batteries. *Angew. Chem. Int. Ed.* **53**, 3096–3101 (2014).
12. Mei, J., Diao, Y., Appleton, A. L., Fang, L. & Bao, Z. Integrated Materials Design of Organic Semiconductors for Field-Effect Transistors. *J. Am. Chem. Soc.* **135**, 6724–6746 (2013).
13. Dai, G. *et al.* Dianthraceno[a,e]pentalenes: synthesis, crystallographic structures and applications in organic field-effect transistors. *Chem. Commun.* **51**, 503–506 (2015).
14. Liu, C. *et al.* Diaceno[a,e]pentalenes: An Excellent Molecular Platform for High-Performance Organic Semiconductors. *Chem. – Eur. J.* **21**, 17016–17022 (2015).
15. Clair, S. & de Oteyza, D. G. Controlling a Chemical Coupling Reaction on a Surface: Tools and Strategies for On-Surface Synthesis. *Chem. Rev.* **119**, 4717–4776 (2019).

16. Shen, Q., Gao, H.-Y. & Fuchs, H. Frontiers of on-surface synthesis: From principles to applications. *Nano Today* **13**, 77–96 (2017).

17. Urgel, J. I. *et al.* On-Surface Synthesis of Heptacene Organometallic Complexes. *J. Am. Chem. Soc.* **139**, 11658–11661 (2017).

18. Zugermeier, M. *et al.* On-surface synthesis of heptacene and its interaction with a metal surface. *Nanoscale* (2017).

19. Zuzak, R. *et al.* Higher Acenes by On-Surface Dehydrogenation: From Heptacene to Undecacene. *Angew. Chem. Int. Ed.* **57**, 10500–10505 (2018).

20. Urgel, J. I. *et al.* On-surface light-induced generation of higher acenes and elucidation of their open-shell character. *Nat. Commun.* **10**, 1–9 (2019).

21. Krüger, J. *et al.* Decacene: On-Surface Generation. *Angew. Chem. Int. Ed.* **56**, 11945–11948 (2017).

22. Eisenhut, F. *et al.* Dodecacene Generated on Surface: Reopening of the Energy Gap. *ACS Nano* **14**, 1011–1017 (2020).

23. Eimre, K. *et al.* On-surface synthesis and characterization of nitrogen-substituted undecacenes. *Nat. Commun.* **13**, 511 (2022).

24. Mishra, S. *et al.* Tailoring Bond Topologies in Open-Shell Graphene Nanostructures. *ACS Nano* **12**, 11917–11927 (2018).

25. Rogers, C. *et al.* Closing the Nanographene Gap: Surface-Assisted Synthesis of Peripentacene from 6,6′-Bipentacene Precursors. *Angew. Chem. Int. Ed.* **54**, 15143–15146 (2015).

26. Sánchez-Grande, A. *et al.* Unravelling the Open-Shell Character of Peripentacene on Au(111). *J. Phys. Chem. Lett.* **12**, 330–336 (2021).

27. Biswas, K. *et al.* Synthesis and Characterization of peri-Heptacene on a Metallic Surface. *Angew. Chem. Int. Ed.* **61**, e202114983 (2022).

28. Majzik, Z. *et al.* Studying an antiaromatic polycyclic hydrocarbon adsorbed on different surfaces. *Nat. Commun.* **9**, 1198 (2018).

29. Di Giovannantonio, M. & Fasel, R. On-surface synthesis and atomic scale characterization of unprotected indenofluorene polymers. *J. Polym. Sci.* **60**, 1814–1826 (2022).

30. Su, J., Telychko, M., Song, S. & Lu, J. Triangulenes: From Precursor Design to On-Surface Synthesis and Characterization. *Angew. Chem. Int. Ed.* **59**, 7658–7668 (2020).

31. Dong, L., Liu, P. N. & Lin, N. Surface-Activated Coupling Reactions Confined on a Surface. *Acc. Chem. Res.* **48**, 2765–2774 (2015).

32. Kinikar, A. *et al.* On-surface polyarylene synthesis by cycloaromatization of isopropyl substituents. *Nat. Synth.* **1**, 289–296 (2022).

33. Biswas, K. *et al.* Interplay between π-Conjugation and Exchange Magnetism in One-Dimensional Porphyrinoid Polymers. *J. Am. Chem. Soc.* **144**, 12725–12731 (2022).

34. Shiotari, A. *et al.* Strain-induced skeletal rearrangement of a polycyclic aromatic hydrocarbon on a copper surface. *Nat. Commun.* **8**, 16089 (2017).

35. Lohr, T. G. *et al.* On-Surface Synthesis of Non-Benzenoid Nanographenes by Oxidative Ring-Closure and Ring-Rearrangement Reactions. *J. Am. Chem. Soc.* **142**, 13565–13572 (2020).

36. Mallada, B. *et al.* On-Surface Strain-Driven Synthesis of Nonalternant Non-Benzenoid Aromatic Compounds Containing Four- to Eight-Membered Rings. *J. Am. Chem. Soc.* **143**, 14694–14702 (2021).

37. Stetsovych, O. *et al.* From helical to planar chirality by on-surface chemistry. *Nat. Chem.* **9**, 213–218 (2017).

38. Albrecht, F. *et al.* Selectivity in single-molecule reactions by tip-induced redox chemistry. *Science* **377**, 298–301 (2022).

39. Cirera, B. *et al.* Thermal selectivity of intermolecular versus intramolecular reactions on surfaces. *Nat. Commun.* **7**, 11002 (2016).

40. Tang, Y. *et al.* On-Surface Debromination of 2,3-Bis(dibromomethyl)- and 2,3-Bis(bromomethyl)naphthalene: Dimerization or Polymerization? *Angew. Chem. Int. Ed.* **n/a**, e202204123.

41. Kawai, S. *et al.* Competing Annulene and Radialene Structures in a Single Anti-Aromatic Molecule Studied by High-Resolution Atomic Force Microscopy. *ACS Nano* **11**, 8122–8130 (2017).

42. Kawai, S. *et al.* An Endergonic Synthesis of Single Sondheimer–Wong Diyne by Local Probe Chemistry. *Angew. Chem. Int. Ed.* **59**, 10842–10847 (2020).

43. Li, D.-Y. *et al.* Ladder Phenylenes Synthesized on Au(111) Surface via Selective [2+2] Cycloaddition. *J. Am. Chem. Soc.* **143**, 12955–12960 (2021).

44. Jacobse, P. H. *et al.* Pseudo-atomic orbital behavior in graphene nanoribbons with four-membered rings. *Sci. Adv.* **7**, eabl5892 (2021).

45. Di Giovannantonio, M. *et al.* On-Surface Synthesis of Antiaromatic and Open-Shell Indeno[2,1-b]fluorene Polymers and Their Lateral Fusion into Porous Ribbons. *J. Am. Chem. Soc.* **141**, 12346–12354 (2019).

46. de la Torre, B. *et al.* Tailoring π-conjugation and vibrational modes to steer on-surface synthesis of pentalene-bridged ladder polymers. *Nat. Commun.* **11**, 4567 (2020).

47. Liu, M. *et al.* Graphene-like nanoribbons periodically embedded with four- and eight-membered rings. *Nat. Commun.* **8**, 14924 (2017).

48. Sánchez-Sánchez, C. *et al.* On-Surface Synthesis and Characterization of Acene-Based Nanoribbons Incorporating Four-Membered Rings. *Chem. – Eur. J.* **25**, 12074–12082 (2019).

49. Fan, Q. *et al.* Nanoribbons with Nonalternant Topology from Fusion of Polyazulene: Carbon Allotropes beyond Graphene. *J. Am. Chem. Soc.* **141**, 17713–17720 (2019).
50. Sánchez-Grande, A. *et al.* On-Surface Synthesis of Ethynylene-Bridged Anthracene Polymers. *Angew. Chem.* **131**, 6631–6635 (2019).
51. Cirera, B. *et al.* Tailoring topological order and π-conjugation to engineer quasi-metallic polymers. *Nat. Nanotechnol.* **15**, 437–443 (2020).
52. Sánchez-Grande, A. *et al.* Diradical Organic One-Dimensional Polymers Synthesized on a Metallic Surface. *Angew. Chem. Int. Ed.* **59**, 17594–17599 (2020).
53. Biswas, K. *et al.* On-surface synthesis of doubly-linked one-dimensional pentacene ladder polymers. *Chem. Commun.* **56**, 15309–15312 (2020).
54. Martín-Fuentes, C. *et al.* Cumulene-like bridged indeno[1,2-b]fluorene π-conjugated polymers synthesized on metal surfaces. *Chem. Commun.* **57**, 7545–7548 (2021).
55. Sánchez-Grande, A. *et al.* Surface-Assisted Synthesis of N-Containing π-Conjugated Polymers. *Adv. Sci.* **9**, 2200407.
56. Urgel, J. I. *et al.* On-Surface Synthesis of Cumulene-Containing Polymers via Two-Step Dehalogenative Homocoupling of Dibromomethylene-Functionalized Tribenzoazulene. *Angew. Chem. Int. Ed.* **59**, 13281–13287 (2020).
57. Di Giovannantonio, M. *et al.* On-Surface Growth Dynamics of Graphene Nanoribbons: The Role of Halogen Functionalization. *ACS Nano* **12**, 74–81 (2018).
58. Di Giovannantonio, M. *et al.* On-Surface Synthesis of Indenofluorene Polymers by Oxidative Five-Membered Ring Formation. *J. Am. Chem. Soc.* **140**, 3532–3536 (2018).
59. Gross, L., Mohn, F., Moll, N., Liljeroth, P. & Meyer, G. The Chemical Structure of a Molecule Resolved by Atomic Force Microscopy. *Science* **325**, 1110–1114 (2009).

60. Hapala, P. *et al.* Mechanism of high-resolution STM/AFM imaging with functionalized tips. *Phys. Rev. B* **90**, 085421 (2014).

61. Zhang, H. *et al.* On-Surface Synthesis of Rylene-Type Graphene Nanoribbons. *J. Am. Chem. Soc.* **137**, 4022–4025 (2015).

62. Zhang, H. *et al.* Surface Supported Gold–Organic Hybrids: On-Surface Synthesis and Surface Directed Orientation. *Small* **10**, 1361–1368 (2014).

63. Levi, Z. U. & Tilley, T. D. Synthesis and Electronic Properties of Extended, Fused-Ring Aromatic Systems Containing Multiple Pentalene Units. *J. Am. Chem. Soc.* **132**, 11012–11014 (2010).

64. Sekine, K. *et al.* Gold-Catalyzed Facile Synthesis and Crystal Structures of Benzene-/Naphthalene-Based Bispentalenes as Organic Semiconductors. *Chem. – Eur. J.* **25**, 216–220 (2019).

65. Tavakkolifard, S. *et al.* Gold-Catalyzed Regiospecific Annulation of Unsymmetrically Substituted 1,5-Diynes for the Precise Synthesis of Bispentalenes. *Chem. – Eur. J.* **25**, 12180–12186 (2019).

66. Frederickson, C. K., Zakharov, L. N. & Haley, M. M. Modulating Paratropicity Strength in Diareno-Fused Antiaromatics. *J. Am. Chem. Soc.* **138**, 16827–16838 (2016).

67. Wilbuer, J., Grenz, D. C., Schnakenburg, G. & Esser, B. Donor- and acceptor-functionalized dibenzo[a,e]pentalenes: modulation of the electronic band gap. *Org. Chem. Front.* **4**, 658–663 (2017).

68. Pavliček, N. *et al.* Polyyne formation via skeletal rearrangement induced by atomic manipulation. *Nat. Chem.* **10**, 853–858 (2018).

69. Giessibl, F. J. Atomic resolution on Si(111)-(7×7) by noncontact atomic force microscopy with a force sensor based on a quartz tuning fork. *Appl. Phys. Lett.* **76**, 1470–1472 (2000).

70. Bartels, L. *et al.* Dynamics of Electron-Induced Manipulation of Individual CO Molecules on Cu(111). *Phys. Rev. Lett.* **80**, 2004–2007 (1998).
71. Horcas, I. *et al.* WSXM: A software for scanning probe microscopy and a tool for nanotechnology. *Rev. Sci. Instrum.* **78**, 013705 (2007).
72. Pearlman, D. A. *et al.* AMBER, a package of computer programs for applying molecular mechanics, normal mode analysis, molecular dynamics and free energy calculations to simulate the structural and energetic properties of molecules. *Comput. Phys. Commun.* **91**, 1–41 (1995).
73. Case, D. A. *et al.* The Amber biomolecular simulation programs. *J. Comput. Chem.* **26**, 1668–1688 (2005).
74. Lewis, J. P. *et al.* Advances and applications in the FIREBALL ab initio tight-binding molecular-dynamics formalism. *Phys. Status Solidi B* **248**, 1989–2007 (2011).
75. Mendieta-Moreno, J. I. *et al.* fireball/amber: An Efficient Local-Orbital DFT QM/MM Method for Biomolecular Systems. *J. Chem. Theory Comput.* **10**, 2185–2193 (2014).
76. Darve, E. & Pohorille, A. Calculating free energies using average force. *J. Chem. Phys.* **115**, 9169–9183 (2001).
77. Izrailev, S. *et al.* Steered Molecular Dynamics. in *Computational Molecular Dynamics: Challenges, Methods, Ideas* (eds. Deuflhard, P. et al.) 39–65 (Springer, 1999).
78. Pastor, R. W., Brooks, B. R. & Szabo, A. An analysis of the accuracy of Langevin and molecular dynamics algorithms. *Mol. Phys.* **65**, 1409–1419 (1988).
79. WHAM – Grossfield Lab. http://membrane.urmc.rochester.edu/?page_id=126.
80. Kumar, S., Rosenberg, J. M., Bouzida, D., Swendsen, R. H. & Kollman, P. A. THE weighted histogram analysis method for free-energy calculations on biomolecules. I. The method. *J. Comput. Chem.* **13**, 1011–1021 (1992).

81. Krejčí, O., Hapala, P., Ondráček, M. & Jelínek, P. Principles and simulations of high-resolution STM imaging with a flexible tip apex. *Phys. Rev. B* **95**, 045407 (2017).
82. Herges, R. & Geuenich, D. Delocalization of Electrons in Molecules [†]. *J. Phys. Chem. A* **105**, 3214–3220 (2001).
83. Chen, Z., Wannere, C. S., Corminboeuf, C., Puchta, R. & Schleyer, P. von R. Nucleus-Independent Chemical Shifts (NICS) as an Aromaticity Criterion. *Chem. Rev.* **105**, 3842–3888 (2005).
84. M. J. Frisch, G. W. Trucks, H. B. Schlegel, G. E. Scuseria, M. A. Robb, J. R. Cheeseman, G. Scal-mani, V. Barone, G. A. Petersson, H. Nakatsuji, X. Li, M. Caricato, A. V. Marenich, J. Bloino, B. G. Janesko, R. Gomperts, B. Mennucci, H. P. Hratchian, J. V. Gaussian 16, Revision C.01. *Gaussian, Inc., Wallingford CT* (2016).
85. Weigend, F. & Ahlrichs, R. Balanced basis sets of split valence, triple zeta valence and quadruple zeta valence quality for H to Rn: Design and assessment of accuracy. *Phys. Chem. Chem. Phys.* **7**, 3297 (2005).